



Contribution Assessment of Northern Hemispheric Atmospheric Circulations to Korean Mid-Summer Surface Warming by the Atmospheric Nudging Experiment

Min-Hee Lee¹ · El Noh^{1,2} · Joo-Hong Kim¹ · Joowan Kim² · Sang-Yoon Jun¹

Received: 31 May 2023 / Revised: 9 August 2023 / Accepted: 22 September 2023
© The Author(s) 2023

Abstract

Anomalous surface warming in Korea has been explained by the high-pressure anomaly accompanied by the vertical sinking motion and weakening of westerlies at the exit of the East Asian Jet. The large-scale circulations linked to this high pressure over East Asia are characterized by the low pressure over the Arctic (AC) and the high pressure over Western Europe (WE), East Asia, and the North Pacific (NP). To assess the contribution of these circulation anomalies to the hot summer in Korea, the four nudging experiments (AC, NP, AC + NP, and WE) are applied to the simulations with 50 different initial conditions in July. As a result, the most similar patterns on local and hemispheric scales are found in the AC + NP nudging experiment. However, the near-surface response in the AC + NP is still weak, and its center shifts to the north compared to the observed, which is induced by the weaker diabatic contribution for the downward motion in the nudging experiment. Using the quasi-geostrophic omega equation, we find that the simulated radiative feedback process is not sufficient to build up the large-scale subsidence with the short nudging period. Despite this limitation, AC + NP well simulates the coherent sinking motion and high-pressure system near Korea by the vorticity advection associated with the upper-level westerlies. It implies that the contribution of the North Pacific circulation (a downstream region) should also be considered to reasonably simulate the East Asia surface warming along with those in the upstream regions.

Keywords Korean summer warming · Atmospheric nudging experiments · Heatwave · Atmospheric teleconnection

1 Introduction

Due to the climate change represented by global warming, more severe cold events in winter and more extreme hot events in summer tend to occur, causing public concern (Alexander et al. 2006; Peterson and Manton 2008; Hansen et al. 2010; Rahmstorf and Coumou 2011; Seneviratne et al. 2014). The frequent occurrence of such extraordinary conditions inevitably has a great social, economic, and health-related impact on human societies in adaptation

to the past weather/climate state (Trenberth et al. 2007; Lee et al. 2012). Therefore, the scientific community has been trying to make the most appropriate response through the prediction of these phenomena.

In particular, the East Asian region including the Korean peninsula is one of the areas where many studies on severe weather events have been conducted because it has a large population and complex weather and climate under the influence of the monsoon system (Wang et al. 2001; Lee et al. 2012). Typically, hot summer in the region has been explained as being related to the presence of the western North Pacific subtropical high (WNPSH) near the region (Luo and Lau 2017; Gao et al. 2018; Ding et al. 2010; Gong et al. 2004). The anticyclone associated with the WNPSH supplies warm and humid air to the region along their edges, and enhances the solar radiation at the surface of the core region. In addition, it has been reported that the summer East Asia jet stream (EAJS) in the upper troposphere can affect the near-surface air temperature by modulating the

✉ Joowan Kim
joowan.k@gmail.com

✉ Sang-Yoon Jun
syjun@kopri.re.kr

¹ Division of Atmospheric Sciences, Korea Polar Research Institute, 26 Sandomirae-ro, Yeonsu-gu, Incheon, Korea

² Department of Atmospheric Science, Kongju National University, Gongju, Korea

East Asian monsoon activity (Yu et al. 2004; Sun et al. 2008, Wang et al., 2013a, b).

In association with this local anticyclonic circulation, the possible influence of the large-scale circulation patterns has been investigated. Some studies have considered the anticyclone as one of the cores in the horizontal Rossby wave propagation (Enomoto et al. 2003; Lee et al. 2017; Yeh et al. 2018; Xu et al. 2019; Yoon et al. 2020) in the northern hemispheric mid-latitudes such as circumglobal teleconnection (CGT, Ding and Wang 2005), North Atlantic Oscillation (NAO, Gao et al. 2018; Sun 2012). In this case, the waves originate from the heat source from the Indian summer monsoon or the baroclinic instability in the jet exit region of the North Atlantic region. Other studies have attempted to explain the meridional wave propagation originated from convection over the subtropical western Pacific (Lee and Lee 2016; He et al. 2018; Shimpo et al. 2019; Wang et al. 2019; Noh et al. 2021) such as the Pacific-Japan (PJ) pattern (Nitta 1987). Some studies have reported that the Korean heat waves related to this anticyclonic anomaly can be classified into several types including the zonal wave and meridional wave type (Yeo et al. 2019; Kim et al. 2021). Recently, the Arctic is also considered a source region of wave propagation in several studies (Wu and Francis 2019; Kim et al. 2022a, b).

Most atmospheric circulation patterns mentioned above are located in the upstream region of the Korean Peninsula. However, we should note that when a high-pressure anomaly appears in the Korean Peninsula, a significant high-pressure anomaly is also observed in the North Pacific. In previous studies, the high-pressure anomaly in the North Pacific has been considered as one of the cores of CGT (Ding et al. 2010; Lee and Lee 2016; Lee et al. 2017; Deng et al. 2019; Kim et al. 2019; Yeo et al. 2019; Choi et al. 2020), or it has been presumed to play a role in blocking the zonal eastward flow which is dominant in this region (Yoon et al. 2020; Yeh et al. 2018; Min et al. 2020). In the case of the former, it was considered as a core that appeared simultaneously with the anticyclone over the Korean Peninsula, so the contribution of this anticyclone at the downstream region was not dealt with in depth. In the latter case, Yoon et al. (2021) examined the effect of each event using a regional climate model from the synoptic point of view, but studies that have looked at the contribution of the high pressure from the large-scale point of view are rare.

Indeed, the anticyclonic circulation over Korea could result from the aggregation of the spatiotemporal variability of various wave propagation and the background flow mentioned above. Therefore, this study aims to assess the influence of the northern hemispheric atmospheric circulation fields, which constitutes the high-pressure anomaly in the Korean Peninsula. In particular, we explore not only the influence of the upstream region of Korea, as examined

in previous studies, but also the contribution of the downstream regions, such as the northern North Pacific, through the nudging experiment. Detailed data and methods used in this study are presented in Section 2. Section 3 represents the observed characteristics of circulations related to the hot summer in Korea and the results of nudging experiments, their interpretations and limitations. Finally, the summary is given in Section 4.

2 Data and Method

2.1 Data

In this study, the fifth-generation global reanalysis product from ECMWF (ERA5; Hersbach et al. 2020) is used for both the observational analysis and the evaluation of the model experiments. Daily 2-m air temperature (T2m), geopotential height (Z), horizontal (U, V) and vertical winds (as pressure velocity, ω), total cloud concentration (TCC), and net surface shortwave radiation flux (FSNS) at the $1^\circ \times 1^\circ$ horizontal resolution during 1979–2020 are included for the observational analysis. For the nudging experiments, U, V, temperature (T), and Z are used to generate the forcing conditions.

2.2 Model Experiments

We use the Community Earth System Model version 2 (CESM2) to explore the characteristics of atmospheric circulations related to mid-summer East Asian surface warming. The nudging method, which is basically implemented within the Community Atmosphere Model version 6 (CAM6), is conducted to investigate the contribution of the specific atmospheric circulation related to East Asian surface warming. The CAM6 nudging method is implemented as a relaxation tendency between the current model state and a desired target state for the prognostic variables of temperature, zonal wind, meridional wind, and specific humidity. The effectiveness of the nudging method for investigating the contribution of atmospheric circulation to a specific phenomenon has been addressed in previous studies (Jung et al. 2014; Yoon et al. 2021).

We utilize a fully coupled configuration under early 21st-century climate conditions for all experiments. The atmosphere and land surface models use a horizontal resolution of f19 (about 2°), and ocean and sea-ice models use a horizontal resolution of g17 (about 1°). Control simulation is conducted from 1 July to 31 July with 50 different initial conditions taken from pre-performed equilibrium simulation with the same configuration. Additional sensitivity experiments were performed by relaxation toward the atmospheric states generated by adding the monthly mean anomaly to air temperature, zonal and meridional winds at every 6-hourly

snapshot of all ensemble members from the control experiment. The monthly mean anomaly is the composite field when the area mean surface air temperature in the East Asian region (30–40°N, 120–135°E) is warmer than one sigma value (Fig. 1a). The relaxation target value at each time step is calculated by the linear interpolation to the atmospheric states at every 6 h for constraining the model to follow a prescribed path.

The relaxation region of each sensitivity experiment is differently confined based on the 500 hPa geopotential height composite anomaly (Fig. 1e). There are three major regions related to East Asia surface warming; the Arctic (north of 63°N), western Europe (43–61°N, 0–40°E), and the North Pacific (30–60°N, 150°E–150°W). In each sensitivity experiment, the relaxation was carried out only over one of the regions with a smoothing zone of about 2 degrees at the boundaries. The name of the sensitivity experiment indicates the region of relaxation; AC (Arctic), WE (Western Europe), NP (North Pacific). In the AC + NP experiment, particularly, the relaxation was carried out over the Arctic and North Pacific regions simultaneously. This simulation was designed to examine the combined contributions of atmospheric circulations over both regions. All experimental designs are briefly summarized in Table 1.

3 Results

3.1 Large-Scale Circulations Associated with Korean Surface Warming in July

Figure 1a shows the time series of T2m over Korea in July 1979–2020. In the original time series as indicated by the black line, the increasing trend is obvious, except for 1994, a year well-known for experiencing an unprecedented and extremely hot summer (Park and Schubert, 1997). This event set records for both the highest temperatures and longest duration in July (Kim et al. 2019; Yeo et al. 2019), despite the relatively weak magnitude of the expanded Western North Pacific Subtropical High (WNPSH) during that period (Kim et al. 2019; Yeo et al. 2019; Yoon et al. 2020). To focus only on the interannual variation of T2m, the trend is removed from the original one and the five years (i.e., 1981, 1994, 2001, 2013, and 2017 presented by closed blue dots) in which T2m above the one standard deviation (i.e., 0.74) are selected for the high-temperature years (HTY) in this study.

During the HTY, high-temperature anomalies (Fig. 1b) are observed around east China, Japan, and the North Pacific, as well as in Korea. The reduced TCC (Fig. 1c) and the enhanced FSNS (Fig. 1d) are consistently found near the high T2m regions, but the maximum latitude is slightly located at the southern part of them. The notable things in the

circulation fields related to the high T2m over Korea are positive anomalies of Z at 500 hPa (Z500), ω at 500 hPa (ω 500), and negative anomalies of U at 200 hPa (U200) as shown in Fig. 1e–g. Typically, it is common to link the strengthening of Z500 in East Asia (including Korea) with the weakening of U200 in the region. Further, it has been reported that the weakening of U200 can induce the sinking motion (i.e., positive ω 500 anomaly) via the secondary circulation around the exit of the upper-level jet region (Wang et al. 2013a). Thus, the warming over Korea in summer is explained by the enhanced FSNS and the downward motion (adiabatic warming), which is related to the high-pressure anomaly and the associated weakening of U200 as a local process.

We further examined how large-scale circulations contribute to the T2m anomaly over Korea beyond the local process. During HTY, a consistent Z500 pattern characterized by one negative core in the Arctic and three positive cores in western Europe, Korea, and the North Pacific is observed with a large significance. Indeed, these patterns have also been reported in previous studies (Yeo et al. 2019; Yeh et al. 2018; Wu and Francis 2019; Choi et al. 2020; Kim et al. 2022a, b) dealing with heat waves in Korea. The second mode of the empirical orthogonal function (EOF) for the summer 1000–500 hPa thickness and the regressed pattern of Z500 onto its PC time series computed in Wu and Francis (2019) are almost similar to the pattern. They suggested that the enhanced Arctic baroclinicity accompanied by a summer Arctic cold anomaly could contribute to the strengthened and weakened tropospheric westerly over the Arctic and mid-latitudes, respectively, which is related to the decreased frequency of the low-pressure system in the mid-latitudes. For the high pressures in Western Europe, East Asia, and the North Pacific, the roles of CGT (Ding and Wang 2005), NAO (Gao et al. 2018; Sun 2012), and PJ (Noh et al. 2021) are suggested in the previous studies.

Most studies mentioned above have focused on the contribution of the circulations in the upstream region of East Asia. However, it is noteworthy that the high pressure over the North Pacific, the downstream region, also has a clear relationship with HTY, which is comparable to the high pressure on the upstream regions. Thus, we try to investigate the contribution of the circulation anomaly from the downstream region on the warming in Korea as well as those from the upstream regions (i.e., the Arctic, and western Europe). A series of nudging experiments are conducted using the forcing over the regions (shown in Fig. 1e by green boxes) to isolate their impact, and the experiment results are discussed in the next section.

3.2 Contribution of Various Remote Circulations Represented in the Nudging Experiments

Figure 2 shows the ensemble mean responses of T2m, Z500, ω 500, U200, and FSNS from each experiment (i.e., AC,

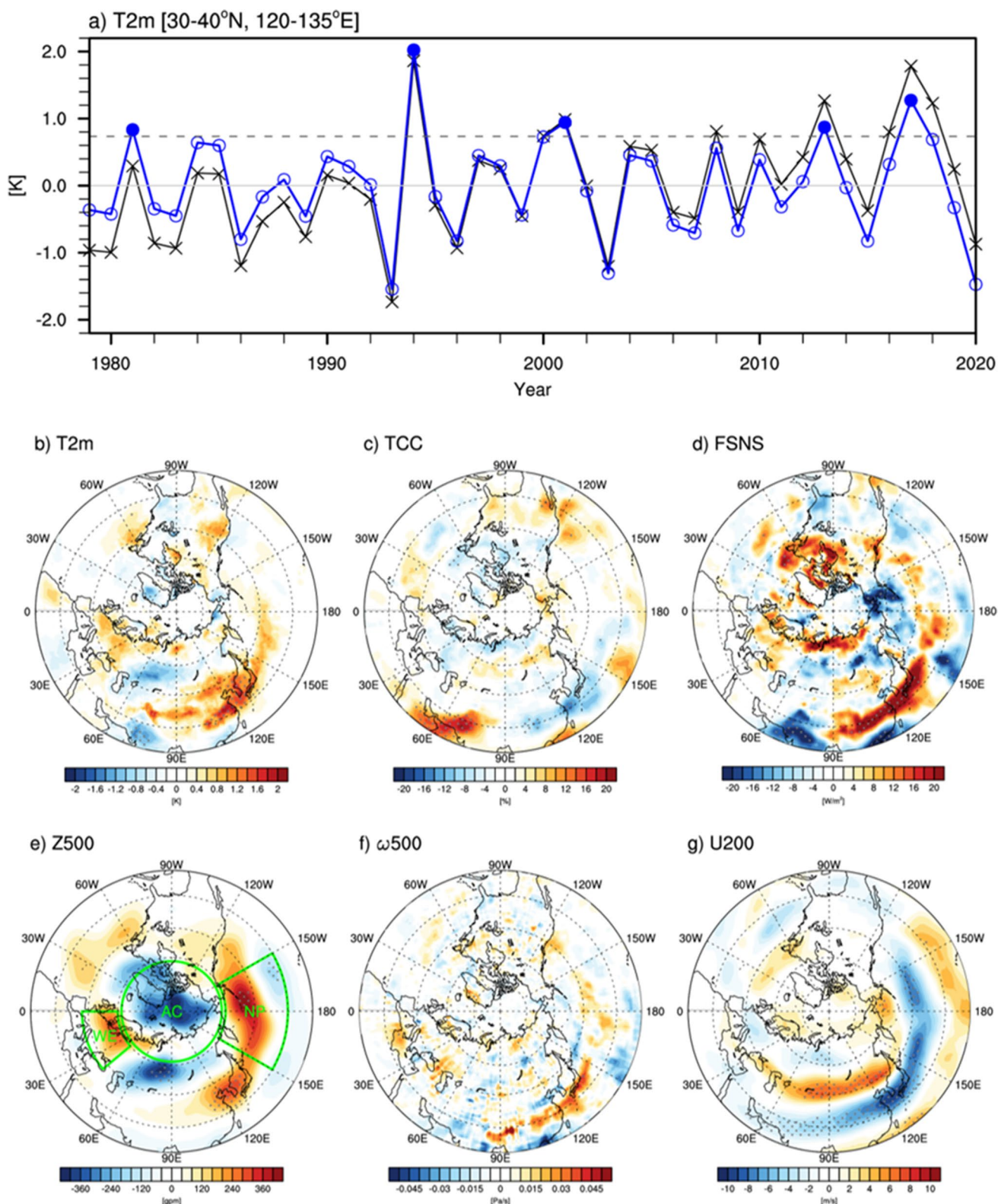


Fig. 1 a) Timeseries (black line and cross mark) and detrended timeseries (blue line and open circle) of T2m around Korea (30–40°N, 120–135°E) in July. Blue closed dots indicate the years show the temperature higher than the 1 standard deviation (i.e., 1981, 1994, 2001,

2013, and 2017). Composite anomalies of **b** T2m, **c** TCC, **d** FSNS, **e** Z500, **f** ω_{500} , **g** U200 during the high temperature years (or hot summer, > 1sigma) in ERA5

Table 1 The relaxation regions of the four different nudging experiments (AC, NP, WE, and AC + NP)

Experiment	Nudging Area
AC	> 63°N
NP	43–61°N, 0–40°E
WE	30–60°N, 150°E–150°W
AC + NP	> 63°N, and 30–60°N, 150°E–150°W

AC + NP, NP, and WE) compared to CTRL. In observation, warm anomalies had already developed from 1 July, whereas the signal in the experiments appeared rather late (Fig. 3), so the composite was conducted based on the values from 8 to 25 July only. Compared to the observational composite, the warm anomaly of T2m tends to be simulated weakly in all experiments. Although AC + NP and NP showed rather higher temperature anomalies in East Asia, the maximum anomaly region was located at a higher latitude of about 5°N compared to those in the observation.

For Z500, the pattern over the Arctic and the Siberian Plain is well simulated in the AC experiment, but the high-pressure pattern over East Asia including Korea and the North Pacific is not well captured. In the WE experiment, a wave-like pattern from western Europe to East Asia via the Ural Mountain is shown, but its intensity is weak. For the NP experiment, although the patterns over western Eurasia and the Arctic are not reproduced, the coherent high-pressure pattern from the Korean Peninsula to the North Pacific appears to be well simulated. It suggests that the high-pressure anomaly existing in the downstream region could also affect the circulation in the upstream region. In the AC + NP experiment, the circulation patterns from the Arctic through the Eurasian continent to the Korean Peninsula and the North Pacific are most similar to the observed patterns. These results imply that while both the AC and WE experiments influence the corresponding wave propagations for the anticyclone in Korea, the intensity of the anticyclone is not sufficiently enhanced without the downstream impact of NP. However, it should be noted that the center of the system locates slightly northward compared to the observation. It seems to be a limitation in the model experiment.

U200 tends to weaken in the south and intensify in the north, based on the region where the high anomalies are shown in Z500. Therefore, in AC and WE, where no clear strengthening of Z500 is observed around Korea and the North Pacific, the weakening of the westerly wind does not clearly appear. However, the AC + NP and NP experiments show strong negative U200 anomalies that are horizontally elongated from Korea to the North Pacific. This anomaly pattern was also reported in previous researches and likely related to the blocking of flow by the persistent anticyclone

over the North Pacific (Yeh et al. 2018; Yoon et al. 2021), while detailed mechanism has not been fully understood.

To examine the daily evolution of variables mentioned above, the time series of each variable averaged around Korea is shown in Fig. 3. For comparison, the time series from the reanalysis (consistent with the pattern in Fig. 1) is also plotted together. It is noted that the cores of anomalies in other variables showing the maximum around Korea (i.e., 30°–40°N, 110°–135°E), except T2m and Z500, are located at the southern part of Korea (i.e., 25°–35°N, 110°–135°E) in observation. The solid black lines in the left panels show the daily climatology of July for each variable averaged over each core region during 1979–2020. The daily evolutions in HFY are displayed as solid red lines. T2m in HFY is already higher than the climatological values from 1 July; this positive anomaly is maintained until the end of July. Z500 in HFY shows a positive value overall compared to the climatology, but it becomes similar to the climatology from around 20 July, which is earlier than the time in T2m. Although ω 500 has a large variability compared to other variables, most of them show values higher than climatology until 28 July, which means that the downward motion is dominant during the period. The variation of FSNS is almost similar to that of ω 500. Like T2m, U200 appears weaker than the climatological values for the entire period, and the difference becomes smaller toward the end of July.

The temporal evolutions of each variable around Korea from each nudging experiment are presented in the middle panel in Fig. 3. Considering that the robust signals in the experiments shifted to the northern area compared to those in observation, all values are averaged at the northern part (i.e., 35°–45°N, 110°–135°E for T2m, Z500, 30°–40°N, 110°–135°E for others as shown in green boxes of Fig. 2) of the area selected for observation. The black line shows the results of CTRL, and the other color lines are the results from various experiments (red, orange, green, and blue lines for AC, AC + NP, NP, and WE, respectively). As expected from the spatial pattern in Fig. 2, the positive anomaly of T2m in all experiments compared to CTRL is not as large as that in the observation. In the observation, the T2m of HFY is larger than the climatology from the first day, whereas T2m in the experiments shows negligible differences during the first 3–5 days. However, it is still noteworthy that the overall positive values of T2m are shown for all experiments. The values in AC + NP (yellow) and NP (yellow-green), are larger than those of other experiments. AC (red) shows a positive value at the beginning, but there is no substantial difference from CTRL afterward, and WE (blue) shows a positive anomaly at the end of July.

Compared to T2m, Z500 has a robust difference between CTRL and other experiments. The largest differences are

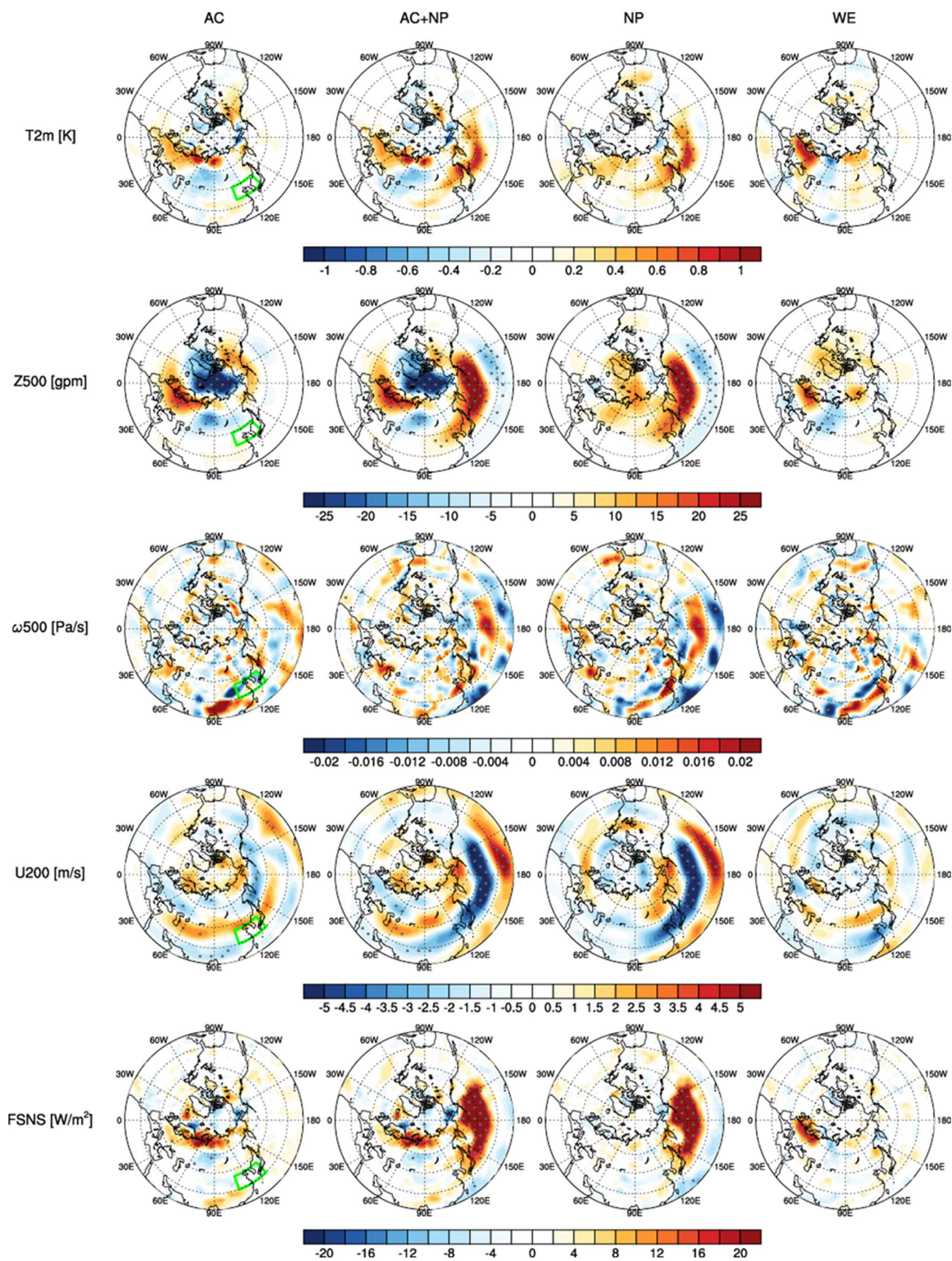


Fig. 2 Anomalies of T2m, TCC, and FSNS for each experiment compared to CTRL during 8–25 days. Green boxes indicate the area selected for the timeseries and bars for experiments in Fig. 3

found in AC + NP and NP as in T2m. Unlike other variables, $\omega 500$ differs greatly in the sign and magnitude of fluctuation depending on the experiment. For example, the result in AC rarely shows higher values compared to CTRL throughout the month, and that in WE presents limited higher values around 15 and 22 July. In the cases of AC + NP and NP, although the variation of $\omega 500$ is relatively large, the overall difference from CTRL tends to be positive. U200 shows mostly weaker values compared to CTRL except for AC. In particular, U200 responses in AC + NP and NP are much stronger for the entire period, and that in WE gets stronger in the later period. FSNS, like in observation, shows variations similar to $\omega 500$. While Z500 and U200 show large anomalies from the beginning period, FSNS shows a notable difference after 10 days.

To summarize the results of the time series discussed above, the values between 8 and 25 days are averaged and expressed as bars in the right panels of Fig. 3. Consistent with the time series, the responses in T2m are relatively weak in all experiments compared to observed anomalies. Although this weak surface warming, regardless of experiments, is a limitation of this study, it is meaningful that AC + NP and NP experiments with relaxation toward anticyclone downstream of Korea make relatively stronger warming than those in AC (Wu and Francis 2019) and WE (Ding and Wang 2005). The anomalies of other circulation fields associated with T2m are well simulated in AC + NP and NP, and the magnitudes are also comparable. In particular, AC + NP with the nudging to both up and downstream of the warming region shows a comprehensive Z500 pattern observed in the northern hemisphere during the HTYs (Fig. 1e). It clearly reproduces the mid-latitude responses over the Eurasian continent. The separate nudging experiments reveal that upstream nudging (AC) is associated with the high and low-pressure dipole over Europe and western Siberia, while downstream nudging (NP) is more closely linked to the high-pressure anomaly over Korea. In addition to these results, the averaged values over the same region as in the observation are also displayed as a dashed bar in the right panel. Since it is not calculated from the maximum response area of the experiments, the overall magnitudes are smaller. However, it can be confirmed that the signs of the differences from CTRL appear consistent.

3.3 Role of the Anomalous High in the North Pacific as a Downstream Circulation

Then, what makes AC + NP most likely to produce results similar to the observations? Based on the results so far, it can be suggested that the key feature for warming in Korea

during summer is the vertical sinking motion associated with the reduced westerlies in the high-pressure anomaly. It is thus important to understand how the vertical structure was constructed in observation and each model experiment and what thermodynamical and dynamical processes contribute to the formation of the vertical structure and motion.

To answer this, we first explore the vertical cross sections of zonally averaged atmospheric fields (U , V , ω , and Z) around Korea (110° – 135° E, Fig. 4). Especially, we try to estimate the contribution of each circulation by comparing AC + NP, which shows the best performance, and AC and NP, which can be regarded as sub experiments of AC + NP. As expected, AC + NP shows the most similarity with the observation. In AC, the negative geopotential anomaly in the Arctic troposphere and the meridional pattern of the associated zonal wind structures match well with those in the observation. However, in the lower latitudes, the signal is only confined to the upper level and does not reach the surface. Conversely, in NP, the patterns of geopotential and zonal wind structures in the south of 50° N shows similar to those in observation, but the pattern in the north is entirely different.

Although the results in AC + NP show structures similar to the observations in general, it still has some differences from the observation. The negative geopotential anomalies over the Arctic tend to be overestimated, and the core of the upper-level zonal wind tends to be weak and spread compared to the observation. The core of the positive geopotential anomaly appears at the lower level in the northern part of the observation, relatively. The associated westerlies and the sinking motion in the mid-latitude tend to be weaker than those in the observation. These differences, which exist even in AC + NP showing the best performance in all nudging experiments, seem to affect a weaker increase in the surface temperature and northerly shifted warming region compared to the observations.

For an in-depth understanding of the processes causing the mid-latitude downward motion in the observations and AC + NP, we explore atmospheric processes related to downward motion with the quasi-geostrophic omega equation. The omega equation is an elliptic diagnostic equation that allows quantitative analysis of forcing mechanisms inducing vertical motion, which include thickness advection, differential of vorticity advection, and diabatic forcing in the atmosphere (cf., Appendix 1 for more detail). The omega equation is solved for a wide region of the East Asian domain, but the vertical motion is analyzed focusing on the downward branch near the Korean Peninsula (30° – 40° N, 110° – 135° E).

Figure 5 presents vertical profiles (Fig. 5a and b) and time series (Fig. 5c and d) of the vertical motion averaged (gray) and computed from the omega equation (black). Despite a notable difference between observed (Fig. 5a, gray) and computed (Fig. 5a, black) vertical velocities due to the quasi-geostrophic approximation and uncertainty in heating rate, the vertical motion from the omega equation shows reasonable

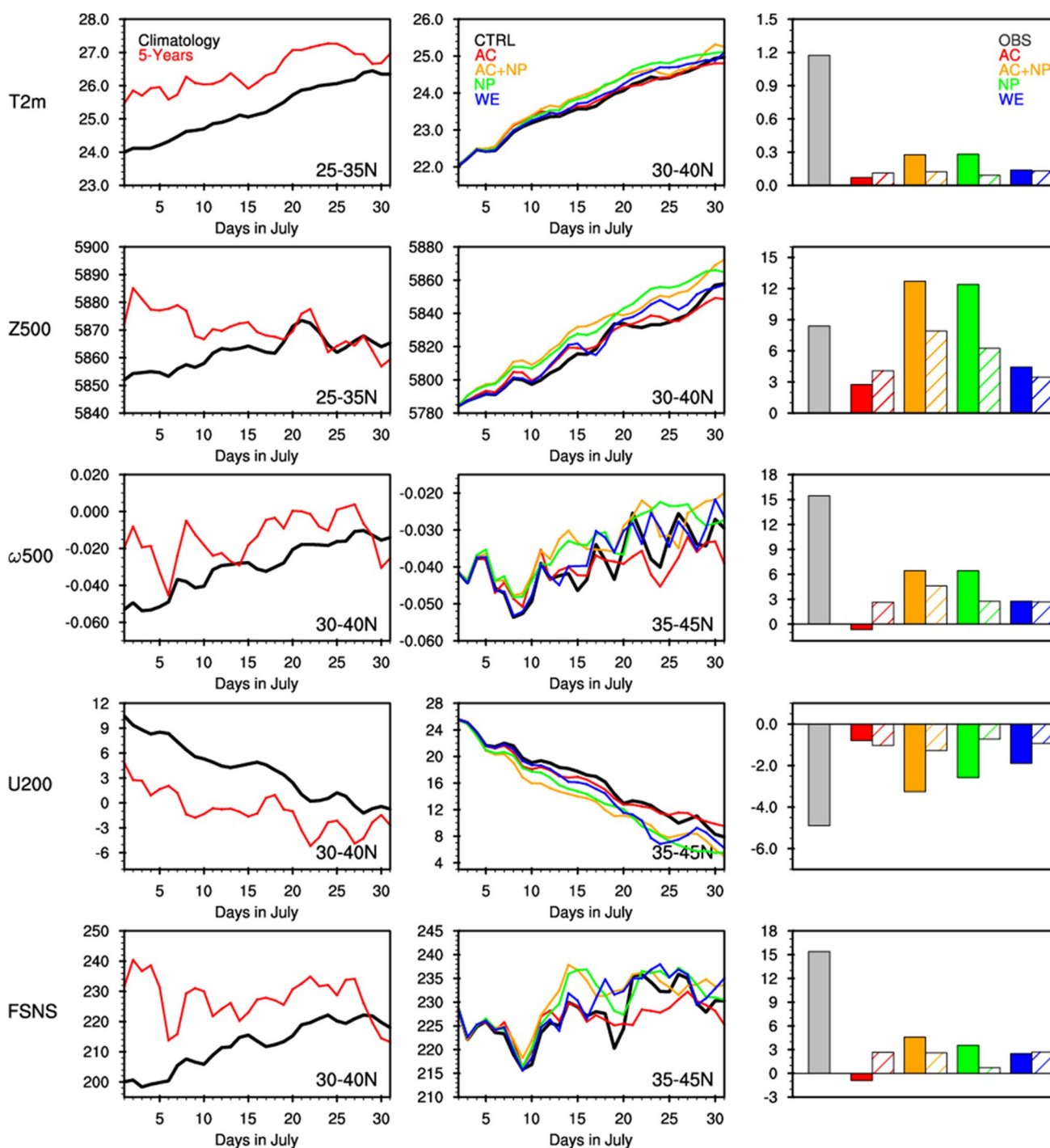


Fig. 3 Timeseries of the averaged at 110–130°E and the latitudinal band represented in each figure for observation (left) and experiments (middle). Bar charts (right) for its averaged values during a certain

period (i.e., July in observation, 8–25 days in experiments). The filled bar and dashed bar show the values averaged at the same area for the observation and experiments, respectively

agreement with the reanalysis in both time series and a vertical structure, showing persistent downward motion centered at ~500 hPa. The linear partitioning by the forcing terms reveals that the primary mechanism of downward motion is the diabatic process (red), which is largely explained by radiative

cooling in this case. Dynamical forcings (temperature and differential vorticity advection) also contribute to the downward motion, while their portions are secondary in this case. A dynamically forced large-scale subsidence can be maintained and further amplified by radiative cooling due to decreased

Fig. 4 Vertical cross-section of zonally averaged geopotential (shading), zonal wind (contour), and meridional-vertical wind (vector) anomalies between 110–135°E

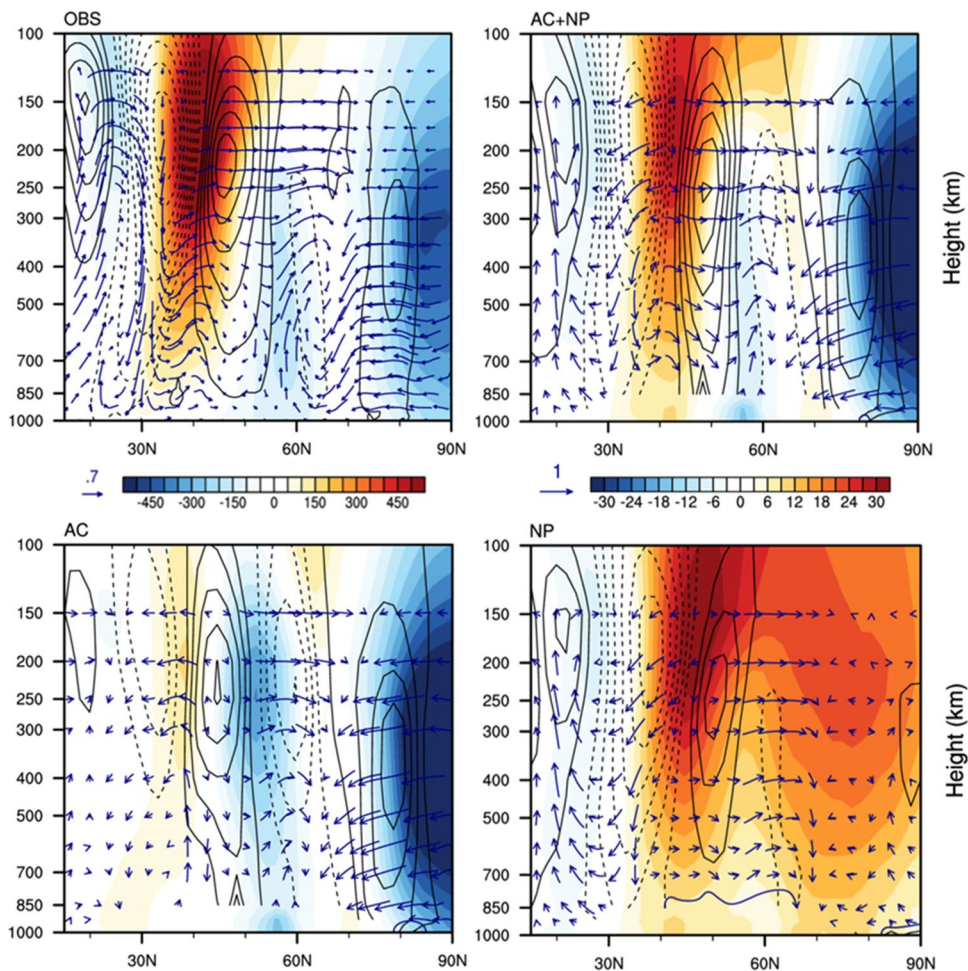
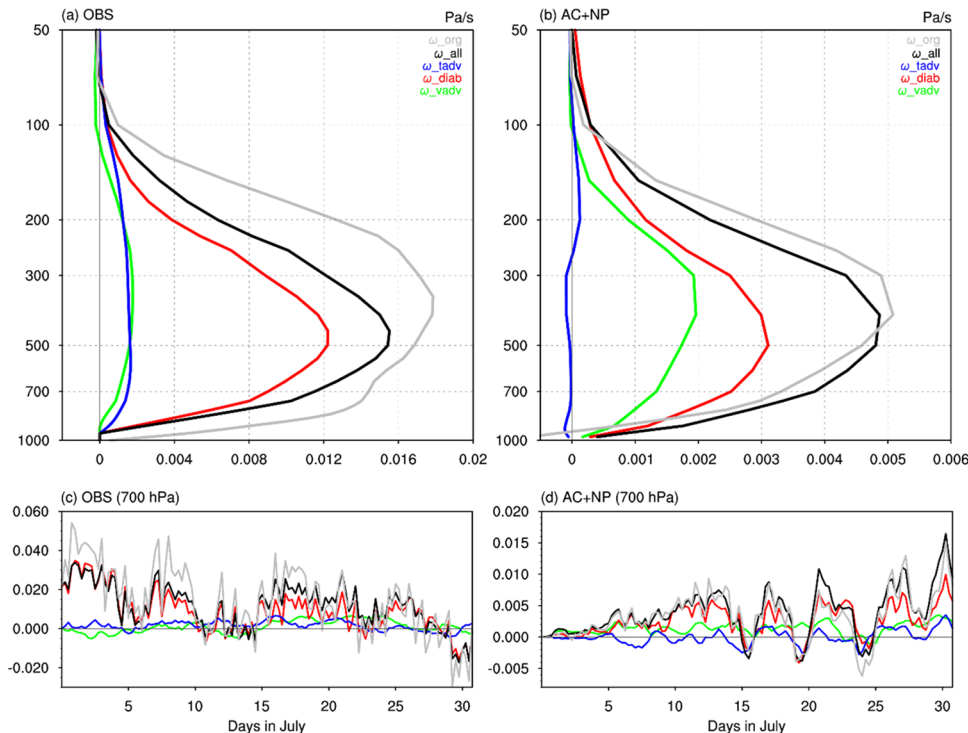


Fig. 5 a, b Vertical profile of the anomalous pressure vertical velocity (gray; Pa s⁻¹) and their partitioning using the omega equation with temperature advection (blue), differential vorticity advection (green), and diabatic forcing (red). The black line presents the sum of all terms in the omega equation for comparison to reanalysis (gray) **c, d** Timeseries of the anomalies at 700 hPa. Left and right columns present reanalysis and AC+NP experiment, respectively



upper-level cloud and increased tropospheric temperature in the subsidence region, which is a radiative feedback observed in deserts (e.g., Rodwell and Hoskins 1996). The subsidence region near Korea also shows a reduction of clouds and increased tropospheric temperature implying the radiation feedback is likely amplifying the coherent high pressure and subsidence patterns observed in July.

A similar temporal and vertical structure of downward motion (Fig. 5b, d) is also found in the AC + NP experiment. It shows a similar magnitude of differential vorticity advection driving downward motion, which is mostly driven by the upper tropospheric circulation pattern. However, the experiment shows a relatively weaker diabatic contribution for the downward motion, which implies that the radiative feedback processes are not sufficiently simulated in the experiment. It could be related to the limited nudging timescale. The radiative feedback on large-scale subsidence generally builds up on seasonal timescales (Hoskins and Rodwell 1995; Rodwell and Hoskins 1996), but the nudging experiments were conducted during a relatively shorter period (one month). The time series (Fig. 5c, d) partly explain the reason for weak diabatic forcing in the model experiment. The reanalysis shows strong diabatic forcing from the beginning of July, suggesting that the radiative impact is already established in advance, while the model's diabatic forcing presents a developing feature during the experiment period. Despite the limitation, the model experiment reveals that the coherent downward motion and high-pressure system near Korea are triggered by the vorticity advection due to upper-level circulation change and are further maintained by radiative feedback in the subsidence region. It is worth noting that the simulated downward motion is also dominated by diabatic forcing after a ramp-up period of one week, which implies that radiative feedback is an important mechanism in maintaining the high-pressure system.

4 Summary and Discussion

This study investigates the contributions of northern hemisphere atmospheric circulations to the East Asian warming in July by nudging experiments of a global climate model. Observational analysis reveals that mid-summer East Asian surface warming is linked to the development of local anticyclonic circulation, which is likely related to atmospheric circulation changes over the Arctic (AC), Western Europe (WE), and the North Pacific (NP). In the nudging experiments (AC, NP, AC + NP, and WE), the circulation changes in the upstream regions (the Arctic and Western Europe) induce weak anticyclonic circulation over East Asia through Rossby wave trains over the Eurasian continent. In addition, the circulation change in the downstream region (the North Pacific) also affects the temperature in

East Asia. Particularly, it alters the downward motion in the mid to upper troposphere over East Asia, which is an essential feature of the Korean mid-summer warming. Namely, the nudging experiment is suggestive of the role of the North Pacific circulation in the warming process of the Korean peninsula. This result is consistent with the other modeling study using a regional model (Yoon et al. 2021).

Although the nudging experiment successfully reproduces the middle to upper tropospheric circulation response over East Asia to the North Pacific circulation change observed in July warming cases, the modeled center of near-surface warming slightly shifts to the north compared to the observation. As mentioned in the result, the observed warming in July is likely accumulated from June with persisting downward shortwave radiation to the surface (Fig. 3), while the nudging experiments are integrated from 1 July. Different initial states and uncertainty in physical parameterizations may have limited the modeled near-surface atmospheric response over East Asia, missing the positive feedback mechanism for the observed surface warming (e.g., Rodwell and Hoskins 1996). Complex land-sea fraction around the Korean Peninsula due to coarse resolution also might weaken the response from the surface (Chou 2003; Okajima et al. 2018). In addition, this study focuses only on July due to the high computational cost of the ensemble experiment. While the key findings of the study are not significantly affected by the chosen period, further investigation in August could be useful considering that heat waves in August are also an important issue in East Asia. Slightly different background conditions and a potential interaction with Tibetan high could be intriguing topics for the heat wave research.

The atmospheric circulations reaching across the Arctic, Eurasia, and Pacific regions in July warming cases suggest the possible linkage among the patterns through the Rossby wave train, such as the CGT pattern (Yeh et al. 2018; Xu et al. 2019; Kim et al. 2022a, b). However, the nudging experiments do not reproduce the linkage among the circulations. The response over the Eurasian continent from the WE experiment is similar to the Scandinavian pattern, but no extension of the pattern is produced in the North Pacific region. Similarly, the AC experiment generates only a weak anticyclonic response confined to the northern boundary of the Bering Sea. The supplementary experiment with anticyclonic nudging over East Asia does not produce the anticyclonic response over the North Pacific (figure not shown), while the anticyclonic nudging over the North Pacific clearly produces the East Asian anticyclone (Fig. 2). Considering the potential contribution of the North Pacific circulation to East Asian weather pattern, which is reported in the literature (Yoon et al. 2020, 2021; Kim et al. 2022a, b) and tested in this paper, further studies are required to better understand the mechanisms of East Asia surface warming associated with the North Pacific region.

Appendix 1: The Omega Budget Equation

The quasi-geostrophic vertical motion equation is obtained by combining the local time derivative vorticity advection, thermodynamic equations, and diabatic heating (Trenberth and Neale, 1977). The equation can be expressed as:

$$\sigma \left(\nabla^2 + \frac{f_0^2}{\sigma} \frac{\partial^2}{\partial p^2} \right) \omega = f_0 \frac{\partial}{\partial p} \left[\vec{V}_g \cdot \nabla (\zeta_g + f) \right] + \nabla^2 \left[\vec{V}_g \cdot \nabla \left(-\frac{\partial \phi}{\partial p} \right) \right] - \frac{R_d}{p} \nabla_p^2 \left(\frac{J}{c_p} \right) \quad (1)$$

where, ω , \vec{V} , and ϕ represent the omega, the horizontal components of velocity, and geopotential, respectively. ζ , f , σ , and R_d are the relative vorticity, planetary vorticity, static stability, and dry air gas constant, respectively, with the suffix “g” indicating geostrophic quantity over the troposphere.

The left-hand side of the equation involves a three-dimensional Laplacian operating on omega and is approximately equivalent to omega multiplied by a negative coefficient. The right-hand side represents the forcing function for omega and consists of differential vorticity advection, thickness advection, and diabatic forcing.

Acknowledgements We thank the two anonymous reviewers for their thoughtful comments and suggestions. This work was funded by the Ministry of Oceans and Fisheries, Korea project entitled ‘Investigation and Prediction System Development of Marine Heatwave around the Korean Peninsula originated from the Sub-Arctic and Western Pacific’ (20190344) and the Korea Polar Research Institute project entitled ‘Development and Application of the Earth System Model-based Korea Polar Prediction System (KPOPS-Earth) for the Arctic and Midlatitude High-impact Weather Events’ (PE23010).

Data Availability The ERA5 data is available at the ECMWF (<https://www.ecmwf.int/en/forecasts/dataset/ecmwf-reanalysis-v5>). The modeling result is available from the corresponding author upon reasonable request.

Declarations

Conflict of Interest The authors declare that they have no conflict of interest.

Open Access This article is licensed under a Creative Commons Attribution 4.0 International License, which permits use, sharing, adaptation, distribution and reproduction in any medium or format, as long as you give appropriate credit to the original author(s) and the source, provide a link to the Creative Commons licence, and indicate if changes were made. The images or other third party material in this article are included in the article’s Creative Commons licence, unless indicated otherwise in a credit line to the material. If material is not included in the article’s Creative Commons licence and your intended use is not permitted by statutory regulation or exceeds the permitted use, you will need to obtain permission directly from the copyright holder. To view a copy of this licence, visit <http://creativecommons.org/licenses/by/4.0/>.

References

- Alexander, L.V., Zhang, X., Peterson, T.C., Caesar, J., Gleason, B., Klein Tank, A.M.G., Haylock, M., Collins, D., Trewin, B., Rahimzadeh, F., Tagipour, A., Kumar, R., Revadekar, K., Griffiths, J., Vincent, G., Stephenson, L., Burn, D.B., Aguilar, J., Brunet, E., Taylor, M., New, M., Zhai, M., Rusticucci, P., Vazquez-Aguirre, M.: Global observed changes in daily climate extremes of temperature and precipitation. *J. Geophys. Res. Atmos.* **111**, D05109 (2006)
- Choi, N., Lee, M.-I., Cha, D.-H., Lim, Y.-K., Kim, K.-M.: Decadal changes in the interannual variability of heat waves in East Asia caused by atmospheric teleconnection changes. *J. Clim.* **33**, 1505–1522 (2020)
- Chou, C.: Land-sea heating contrast in an idealized asian summer monsoon. *Clim. Dyn.* **21**, 11–25 (2003)
- Deng, K., Yang, S., Lin, A., Li, C., Hu, C.: Unprecedented east asian warming in spring 2018 linked to the North Atlantic tripole SST mode. *Atmos. Ocean Sci. Lett.* **12**(4), 246–253 (2019)
- Ding, T., Qian, W., Yan, T.: Changes in hot days and heat waves in China during 1961–2007. *Int. J. Climatol.* **30**(10), 1452–1462 (2010)
- Ding, Q., Wang, B.: Circumglobal teleconnection in the Northern Hemisphere summer. *J. Clim.* **18**(21), 3483–3505 (2005)
- Enomoto, T., Hoskins, B.J., Matsuda, Y.: The formation mechanism of the Bonin high in August. *Q. J. R. Meteorol. Soc.* **129**(587), 157–178 (2003)
- Gao, M., Wang, B., Yang, J., Dong, W.: Are peak summer sultry heat wave days over the Yangtze-Huaihe River basin predictable? *J. Clim.* **31**(6), 2185–2196 (2018)
- Gong, D., Wang, S., Wang, J.: Changes in extreme daily mean temperatures in summer in eastern China during 1955–2000. *Theor. Appl. Climatol.* **77**(1–2), 25–37 (2004)
- Hansen, J., Ruedy, R., Sato, M., Lo, K.: Global surface temperature change. *Rev. Geophys.* **48**(4), RG4004 (2010)
- He, C., Lin, A., Gu, D., Li, C., Zheng, B., Wu, B., Zhou, T.: Using eddy geopotential height to measure the western North Pacific subtropical high in a warming climate. *Theor. Appl. Climatol.* **131**(1–2), 681–691 (2018)
- Hersbach, H., Bell, B., Berrisford, P., Hirahara, S., Horányi, A., Muñoz-Sabater, J., Nicolas, J., Peubey, C., Radu, R., Schepers, D., Simmons, A., Soci, C., Abdalla, S., Abellan, X., Balsamo, G., Bechtold, P., Biavati, G., Bidlot, J., Bonavita, M., De Chiara, G., Dahlgren, P., Dee, D., Diamantakis, M., Dragani, R., Flemming, J., Forbes, R., Fuentes, M., Geer, A., Haimberger, L., Healy, S., Hogan, R.J., Hólm, E., Janisková, M., Keeley, S., Lalouaux, P., Lopez, P., Lupu, C., Radnoti, G., de Rosnay, P., Rozum, I., Vamborg, F., Villaume, S., Thépaut, J.-N.: The ERA5 global reanalysis. *Q. J. R. Meteorol. Soc.* **146**, 1999–2049 (2020)
- Hoskins, B.J., Rodwell, M.J.: A model of the asian summer monsoon. Part I: The global scale. *J. Atmos. Sci.* **52**(9), 1329–1340 (1995)
- Jung, T., Kasper, M.A., Semmler, T., Serrar, S.: Arctic influence on subseasonal midlatitude prediction. *Geophys. Res. Lett.* **41**, 3676–3680 (2014)
- Kim, J.-H., Kim, S.-J., Kim, J.-H., Hayashi, M., Kim, M.-K.: East asian heat waves driven by Arctic-Siberian warming. *Sci. Rep.* **12**, 18025 (2022a)
- Kim, D.S., Jun, S.Y., Lee, M.I., Kug, J.S.: Significant relationship between Arctic warming and East Asia hot summers. *Int. J. Climatol.* **42**(16), 9530–9538 (2022b)
- Kim, H.-K., Moon, B.-K., Kim, M.-K., Park, J.-Y., Hyun, Y.-K.: Three distinct atmospheric circulation patterns associated with high temperature extremes in South Korea. *Sci. Rep.* **11**, 12911 (2021)
- Kim, M.-K., Oh, J.-S., Park, C.-K., Min, S.-K., Boo, K.-O., Kim, J.-H.: Possible impact of the diabatic heating over the indian

- subcontinent on heat waves in South Korea. *Int. J. Climatol.* **39**, 1166–1180 (2019)
- Lee, M.-H., Ho, C.-H., Kim, J., Song, C.-K.: Assessment of the changes in extreme vulnerability over East Asia due to global warming. *Clim. Change* **113**, 301–321 (2012)
- Lee, W., Lee, M.: Interannual variability of heat waves in South Korea and their connection with large-scale atmospheric circulation patterns. *Int. J. Climatol.* **36**(15), 4815–4830 (2016)
- Lee, M.-H., Lee, S., Song, H.-J., Ho, C.-H.: Recent shift in sub-seasonal boreal summer teleconnection and its influence on temperature extremes. *J. Clim.* **30**, 7493–7504 (2017)
- Luo, M., Lau, N.-C.: Heat waves in southern China: Synoptic behavior, long-term change and urbanization effects. *J. Clim.* **30**, 703–720 (2017)
- Min, K.-H., Chung, C.H., Bae, J.H., Cha, D.H.: Synoptic characteristics of extreme heatwaves over the Korean Peninsula based on ERA interim reanalysis data. *Int. J. Climatol.* **40**, 3179–3195 (2020)
- Nitta, T.: Convective activities in the Tropical Western Pacific and their impact on the northern hemisphere summer circulation. *J. Meteorol. Soc. Japan Ser. II* **65**(3), 373–390 (1987)
- Noh, E., Kim, J., Jun, S.-Y., Cha, D.-H., Park, M.-S., Kim, J.-H., Kim, H.-G.: The role of the Pacific-Japan pattern in extreme heatwaves over Korea and Japan. *Geophys. Res. Lett.* **48**, e2021GL093990 (2021)
- Okajima, S., Nakamura, H., Nishii, K., Miyasaka, T., Kuwano-Yoshida, A., Taguchi, B., Mori, M., Kosaka, Y.: Mechanisms for the maintenance of the wintertime basin-scale atmospheric response to decadal SST variability in the North Pacific subarctic frontal zone. *J. Clim.* **31**(1), 297–315 (2018)
- Park, C.-K., and Schubert, S. D.: On the Nature of the 1994 East Asian Summer Drought. *J. Climate.* **10**(5), 1056–1070 (1997). [https://doi.org/10.1175/1520-0442\(1997\)0102.0.CO;2](https://doi.org/10.1175/1520-0442(1997)0102.0.CO;2)
- Peterson, T.C., Manton, M.J.: Monitoring changes in climate extremes: A tale of international collaboration. *Bull. Am. Meteorol. Soc.* **89**, 1266–1271 (2008)
- Rahmstorf, S., Coumou, D.: Increase of extreme events in a warming world. *Proc. Natl. Acad. Sci. USA* **108**, 17905–17909 (2011)
- Rodwell, M., Hoskins, J.: Monsoons and the dynamics of deserts. *Q. J. R. Meteorol. Soc.* **122**(534), 1385–1404 (1996)
- Seneviratne, S.I., Donat, M.G., Mueller, B., Alexander, L.V.: No pause in the increase of hot temperature extremes. *Nat. Clim. Change* **4**, 161–163 (2014)
- Shimpo, A., Takemura, K., Wakamatsu, S., Togawa, H., Mochizuki, Y., Takekawa, M., Tanaka, S., Yamashita, K., Maeda, S., Kurora, R., Murai, H., Kitabatake, N., Tsuguti, H., Mukougawa, H., Iwasaki, T., Kawamura, R., Kimoto, M., Takayabu, I., Takayabu, Y.N., Tanimoto, Y., Hirooka, T., Masumoto, Y., Watanabe, M., Tsuboki, K., Nakamura, H.: Primary factors behind the heavy rain event of July 2018 and the subsequent heat wave in Japan. *SOLA* **15A**(A), 13–18 (2019)
- Sun, J.Q.: Possible impact of the summer North Atlantic Oscillation on extreme hot events in China. *Atmos. Ocea Sci. Lett.* **5**(3), 231–234 (2012)
- Sun, J., Wang, H., Jin, W.B.: Recent trends in observed temperature and precipitation extremes in the Yangtze River basin, China. *Theor. Appl. Climatol.* **83**(1–4), 139–151 (2008)
- Trenberth, K. E., and Neale, A. A.: Numerical Weather Prediction in New Zealand. *Mon. Wea. Rev.* **105**(7), 817–825 (1977). [https://doi.org/10.1175/1520-0493\(1977\)1052.0.CO;2](https://doi.org/10.1175/1520-0493(1977)1052.0.CO;2)
- Trenberth, K.E., et al.: Observations: Surface and atmospheric climate change. In: *Climate Change 2007: The Physical Science Basis. Contribution of Working Group I to the Fourth Assessment Report of the Intergovernmental Panel on Climate Change*, Solomon, S. et al. (Eds.), pp. 235–336. Cambridge University Press, Cambridge, UK and New York, USA (2007)
- Wang, S.S.Y., Kim, H., Coumou, D., Yoon, J., Zhao, L., Gillies, R.R.: Consecutive extreme flooding and heat wave in Japan: Are they becoming a norm? *Atmos. Ocea Sci. Lett.* **20**(10), 2–5 (2019)
- Wang, B., Wu, R., Lau, K.: Interannual variability of the asian summer monsoon: Contrasts between the indian and the western North Pacific-East Asian monsoons. *J. Clim.* **14**(20), 4073–4090 (2001)
- Wang, W., Zhou, W., Wang, X., Fong, S.K., Leong, K.C.: Summer high temperature extremes in Southeast China associated with the east asian jet stream and circumglobal teleconnection. *J. Geophys. Res.* **118**, 8306–8319 (2013a)
- Wang, X., Zhou, W., Wang, D., Wang, C.: The impacts of the summer asian jet stream biases on surface air temperature in mid-eastern Cahina in IPCC AR4 models. *Int. J. Climatol.* **33**, 265–276 (2013b)
- Wu, B., Francis, J.A.: Summer Arctic cold anomaly dynamically linked to east asian heat waves. *J. Clim.* **32**, 1137–1150 (2019). <https://doi.org/10.1175/KCLI-D-18-0370.1>
- Xu, P., Wang, L., Chen, W., Feng, J., Liu, Y.: Structural changes in the Pacific-Japan pattern in the late 1990s. *J. Clim.* **32**(2), 607–621 (2019)
- Yeh, S.-W., Won, Y.-J., Hong, J.-S., Lee, K.-J., Kwon, M., Seo, K.-H., Ham, Y.-G.: The record-breaking heat wave in 2016 over South Korea and its physical mechanism. *Mon. Wea. Rev.* **146**(5), 1463–1474 (2018)
- Yeo, S.R., Yeh, S.-W., Lee, W.-S.: Two types of heat wave in Korea associated with atmospheric circulation pattern. *J. Geophys. Res.* **124**(14), 7498–7511 (2019)
- Yeo, S.-R., Yeh, S.-W., Won, Y., Jo, H., Kim, W.: Distinct mechanisms of korean surface temperature variability during early and late summer. *J. Geophys. Res.* **122**, 6137–6151 (2017)
- Yoon, D., Cha, D.-H., Lee, M.-I., Min, K.-H., Jun, S.-Y., Choi, Y.: Comparison of regional climate model performances for different types of heat waves over South Korea. *J. Clim.* **34**(6), 2157–2174 (2021)
- Yoon, D., Cha, D.-H., Lee, M.-I., Min, K.-H., Kim, J., Jun, S.-Y., Choi, Y.: Recent changes in heatwave characteristics over Korea. *Clim. Dyn.* **55**(7–8), 1685–1696 (2020)
- Yu, R., Wang, B., Zhou, T.: Tropospheric cooling and summer monsoon weakening trend over East Asia. *Geophys. Res. Lett.* **31**, L22212 (2004)

Publisher's Note Springer Nature remains neutral with regard to jurisdictional claims in published maps and institutional affiliations.